Metadata of the chapter that will be visualized in SpringerLink

Book Title	50+ Years of AIMETA	
Series Title		
Chapter Title	Stability Analyses to Predict Tidal Sedimentary Patterns	
Copyright Year	2022	
Copyright HolderName	The Author(s), under exclusive license to Springer Nature Switzerland AG	
Corresponding Author	Family Name	**Blondeaux**
	Particle	
	Given Name	**Paolo**
	Prefix	
	Suffix	
	Role	
	Division	
	Organization	University of Genova
	Address	Genova, Italy
	Email	paolo.blondeaux@unige.it
Author	Family Name	**Vittori**
	Particle	
	Given Name	**Giovanna**
	Prefix	
	Suffix	
	Role	
	Division	
	Organization	University of Genova
	Address	Genova, Italy
	Email	giovanna.vittori@unige.it

Abstract	The results on the prediction of (i) the conditions leading to the appearance of periodic sedimentary patterns forced by tidal currents on the sea bottom and (ii) the geometrical characteristics of these bottom forms are summarized. Attention is focused on the results obtained by means of stability analyses, even though a few results obtained by means of numerical simulations are also mentioned. The characteristics of ripples, dunes, sand waves, long bed waves and sand banks are described along with the mechanisms that originate these different sedimentary patterns.

Stability Analyses to Predict Tidal Sedimentary Patterns

Paolo Blondeaux and Giovanna Vittori

The results on the prediction of (i) the conditions leading to the appearance of periodic sedimentary patterns forced by tidal currents on the sea bottom and (ii) the geometrical characteristics of these bottom forms are summarized. Attention is focused on the results obtained by means of stability analyses, even though a few results obtained by means of numerical simulations are also mentioned. The characteristics of ripples, dunes, sand waves, long bed waves and sand banks are described along with the mechanisms that originate these different sedimentary patterns.

1 Introduction

Many sedimentary patterns (bedforms), which can be observed on the continental shelves or on a river bed, are repetitive both in space and time and it is possible to associate to them a characteristic wavelength L^* and a characteristic period T^* (hereinafter a star denotes a dimensional quantity). The reader who is interested in a description of the main characteristics of the bedforms observed on the sea bottom or on a river bed can read the monograph of Blondeaux et al. [6].

Nowadays, it is widely accepted that the appearance of periodic bedforms is due to the instability of the plane interface between the sea/river bottom, made up of cohesionless sediments, and the water flowing over it. Different physical mechanisms are commonly proposed to explain the appearance of the different sedimentary patterns even though, in a recent contribution, Vittori and Blondeaux [35] discussed the theories of formation of river dunes and tidal sand waves and showed that the different physical mechanisms proposed to explain their formation show more similarities than it was believed. Certainly, because of the different length scales, which characterize the different bedforms, different approaches are used to investigate the

P. Blondeaux (✉) · G. Vittori
University of Genova,Genova, Italy
e-mail: paolo.blondeaux@unige.it

G. Vittori
e-mail: giovanna.vittori@unige.it

G. Rega (ed.), *50+ Years of AIMETA*,
https://doi.org/10.1007/978-3-030-94195-6_21

processes that lead to the formation of ripples, megaripples, dunes, bars, sand waves, long bed waves and sand banks.

In the present contribution, we focus our attention on the bedforms that are generated on the continental shelves by the currents forced by tide propagation. Even narrowing the focus on the bedforms generated by tidal currents, the topic is extremely vast and it is not possible to describe in detail the results available in the literature. Consequently, we will limit ourselves to a brief description of the approaches used to study tidal bedforms and a summary of the main results, providing some references, which can be consulted by the reader who wants to deepen the subject.

As already pointed out, the appearance of periodic bedforms is assumed to be the result of the instability of the flat configuration of the sea bottom above which the water flows and induces the sediment motion. The stability of the flat bottom is investigated by determining the time development of a random perturbation of the flat bed. The growth/decay of the bottom perturbation is determined by assuming that its initial amplitude is 'small' and by linearizing the morphodynamic problem. Therefore, it is possible to consider separately the different components of the bottom waviness

$$z^* = \eta^* \left(x^*, y^*, z^*, t^*\right) = \frac{h_0^*}{2} \epsilon A(t^*) \exp\left[i \left(\alpha_x^* x^* + \alpha_y^* y^*\right)\right] + \text{c.c.}. \qquad (1)$$

In (1), (x^*, y^*, z^*) is a Cartesian coordinate system, with the x^*- and y^*-axes lying on the average bottom and the z^*-axis being orthogonal to it and pointing upwards, and h_0^* is the mean water depth. The parameter ϵ is a measure of the ratio between the amplitude of the bottom perturbation and the local water depth and is assumed to be much smaller than one ($\epsilon \ll 1$). Moreover α_x^* and α_y^* are the wavenumbers of the generic component of the bottom waviness and $A(t^*)$, which is assumed to be of order 1, describes the time development of its amplitude (c.c. indicates the complex conjugate of the previous term). The growth of the most unstable component, if any, is assumed to generate the observed bottom forms.

Of course, the bottom waviness induces perturbations of (i) the flow field, (ii) the bottom shear stress and (iii) the (volumetric) sediment transport rate. To determine the time development of the perturbation of the sea bottom, which is supposed to be made of cohesionless sediments of uniform size d^* and density ρ_s^*, it is necessary to determine the flow generated by a tidal current over a wavy bottom, which is assumed to be fixed. Indeed, the time scale T_M^* of the evolution of the bottom perturbation (the morphodynamic time scale) is much longer than the hydrodynamic time scale T_H^*. The different spatial and temporal scales, which characterize the different bedforms, imply the use of different approaches to solve the hydrodynamic problem. In particular, to study the hydrodynamic phenomena that take place in large areas of the Earth surface but characterized by a length scale significantly smaller than the Earth radius, it is appropriate to introduce the f-plane approximation (see for example [21]) and to consider momentum equations where the Coriolis contributions related to the Earth rotation are taken into account.

If the problem is written in dimensionless form using the water depth h_0^*, the inverse of the angular frequency ω^* and the amplitude U_0^* of the velocity oscillations induced by tide propagation as length, time and velocity scales, respectively, four dimensionless parameters appear, which are $\hat{r} = U_0^*/\left(\omega^* h_0^*\right)$, $\hat{\delta} = \sqrt{\nu_{T0}^*/\omega^*}/h_0^*$, $\hat{Fr} = U_0^*/\sqrt{g^* h_0^*}$, $\hat{\Omega} = \Omega^*/\omega^*$. The parameter $\hat{r}$ is the ratio between the amplitude of fluid displacement oscillations in the horizontal direction and the local water depth and it turns out to be order 10^2. The parameter $\hat{\delta}$ is the ratio between the order of magnitude of the thickness of the bottom boundary layer generated by the tidal wave and the local depth and it turns out to be of order one. The Froude number $\hat{Fr}$ can be written as $\left(U_0^*/\omega\right)\left(\omega/\sqrt{g^* h_0^*}\right)$ and can be thought as the ratio between the amplitude of fluid displacement oscillations in the horizontal direction and the order of magnitude of length of the tidal wave. Finally, $\hat{\Omega}$ is the ratio between the angular velocity of the Earth rotation Ω^* and the angular frequency of the tidal wave ($\hat{\Omega} \cong 0.5$ for a semidiurnal tide, $\hat{\Omega} \cong 1$ for a diurnal tide). Often, the problem can be simplified by assuming that the Froude number $\hat{Fr}$ is much smaller than one. Indeed, the assumption $\hat{Fr} \ll 1$ allows the rigid lid approximation to be introduced.

The complete equations are often simplified when large scale bedforms are considered (e.g. long bed waves and sand banks). In this case, the water depth turns out to be much smaller than the wavelength of the bedforms and the shallow water approximation can be introduced. Hence, the depth averaged values of the velocity components can be considered and different dimensionless variables are introduced.

Once the flow field is determined, it is necessary to evaluate the sediment flux. The sediment flux due to the sediments that move close to the bed, rolling, sliding and saltating over the resting bed (bed load) is usually evaluated by means of empirical formulae. The sediment flux due to the sediments that move far from the bottom being trapped within the large scale turbulent vortices (suspended load) is usually evaluated by solving an advection-diffusion equation for the sediment concentration.

Then, mass conservation of the sediments (Exner equation) implies that a spatial increase of the sediment transport rate implies a decrease of the bed elevation and vice versa. This mass balance equation gives rise to an amplitude equation for A which can be written in the form

$$\frac{dA}{dt^*} = \Gamma^* A \tag{2}$$

where $\Gamma^* = \Gamma_r^* + i\Gamma_i^*$ is a complex quantity which depends on both the hydrodynamic and morphodynamic parameters of the problem.

When it is reasonable to consider a steady forcing flow, the value of Γ^* is independent of time and the amplitude equation (2) can be easily integrated. Then, it is straightforward to discriminate between growing ($\Gamma_r^* > 0$) and decaying ($\Gamma_r^* < 0$) components of the bottom perturbation. Moreover, it is possible to determine the orientation and wavelength of the periodic bedforms predicted by the analysis.

However, tide propagation gives rise to a time dependent (periodic) flow and Γ^* turns out to be a periodic function of time. Therefore, different contributions to the time development of $A(t^*)$ can be identified. The most important contributions are

related to the real and imaginary parts of the time average $\overline{\Gamma}^*$ of Γ^* defined by $\overline{\Gamma}^* = \int_0^{T_0^*} \Gamma(\hat{t}^*) d\hat{t}^*$, T_0^* being the period of the tide. The decay/amplification of the bottom waviness is controlled by the value of $\overline{\Gamma}^*{}_r$ while $\overline{\Gamma}^*{}_i$ controls the migration of the bottom forms. The further contributions to $A(t^*)$, which are related to $\Gamma^* - \overline{\Gamma}^*$, describe the oscillations (during the tide period) of the bottom profile around its averaged position. Such oscillations are small and, in general, are not considered.

2 An Overview of the Results of the Stability Analyses

The sedimentary patterns generated by tidal currents are characterized by spatial and temporal scales that range from centimetres to kilometres and from minutes to centuries. Hence, the theoretical models used to investigate the process which leads to the appearance of the different tidal bedforms are based on different approaches. Therefore, in the following, we consider separately the formation of (i) ripples and dunes, (ii) sand waves, (iii) long bed waves and (iv) sand banks, even though the different bedforms may coexist and interact. Since ripples and dunes are characterized by values of the morphodynamics time scale T_M^* that are smaller than the period T_0^* of the tide, they can be assumed to be generated by a steady (slowly variable) current and there is no need to account for the oscillatory character of the tidal current. On the other hand, sand waves, long bed waves and sand banks should be studied taking into account the periodic character of the tidal currents, since the value of T_M^* of these bedforms is larger than T_0^*.

2.1 Ripples and Megaripples/Dunes

Both ripples and megaripples/dunes are small scale undulations of the sea bottom. The first bedforms are characterized by wavelength of the order of tens of centimetres whereas the second bedforms have typical wavelength of the order of metres. As already pointed out, it is reasonable to investigate the process that leads to the formation of the ripples and dunes generated by tidal currents by considering a sequence of steady flows as in [11, 13]. Indeed, the characteristics of the small scale bedforms generated by tidal currents do not significantly differ from those observed along a river course (see Fig. 1).

The hydrodynamic and morphodynamic problems can be solved by expanding any unknown function as a power series of ϵ. This procedure leads to a sequence of problems at the different orders of approximation. At the leading order ($O(\epsilon^0)$), the velocity profile is described by the well known logarithmic law for both the hydraulically rough and smooth regimes. At O(ϵ), an eigenvalue problem was obtained by Colombini and Stocchino [13], who solved it by forcing an eigenrelation which provides the value of Γ^*. Colombini and Stocchino [13] obtained Γ^*

Fig. 1 Ripples on the bottom of the Hunter river (New South Wales, Australia). Current direction is from the top-right to the bottom-left. Photo courtesy of Michael C. Rygel

as a function of the ratio between the Shields parameter and its critical value and the dimensionless wavenumber α, for different values of the sediment Reynolds number $R_p = \sqrt{(\rho_s^*/\rho^* - 1)g^* d^{*3}}/\nu^*$, ρ_s^* and ρ^* being the densities of the sediments and of the water, respectively, g^* the acceleration of gravity, d^* the sediment size and ν^* the kinematic viscosity of the water. Their results, supported by a comparison with the experimental observations described in [16], show that for large values of R_p (e.g. $R_p = 20$), only one unstable region appears for values of α typical of dunes, i.e. α of order 1. For smaller values of R_p ($R_p = 14$), a second unstable region appears for α of order 10. This range of wavenumbers can be related to ripples. When the value of the sediment Reynolds number is further decreased, the two unstable regions merge but two different relative maxima of the growth rate can still be identified down to a value of R_p equal to 10 (see Fig. 2). Then, a further descrease of R_p leads to a single maximum. Of course, the linear approach described in [13] cannot predict if one mode would eventually prevail over the other. However, it is worth pointing out that experimental observations [16] show that ripples and dunes may coexist. Therefore, the results of the analyses described in [11, 13] suggest that ripples and dunes are two different modes that can be excited individually or simultaneously. On the other hand, Fourriere et al. [15] proposed a model that shows that the most unstable wavelength of the bottom perturbations, forced by a uniform steady current, corresponds to ripples. According to Fourriere et al. [15] dunes are the result of a nonlinear process (ripple coarsening). In any case, the physical mechanism which drives the growth of ripples and dunes is the phase shift between the perturbation of the bottom profile and the perturbation of the bed shear stress.

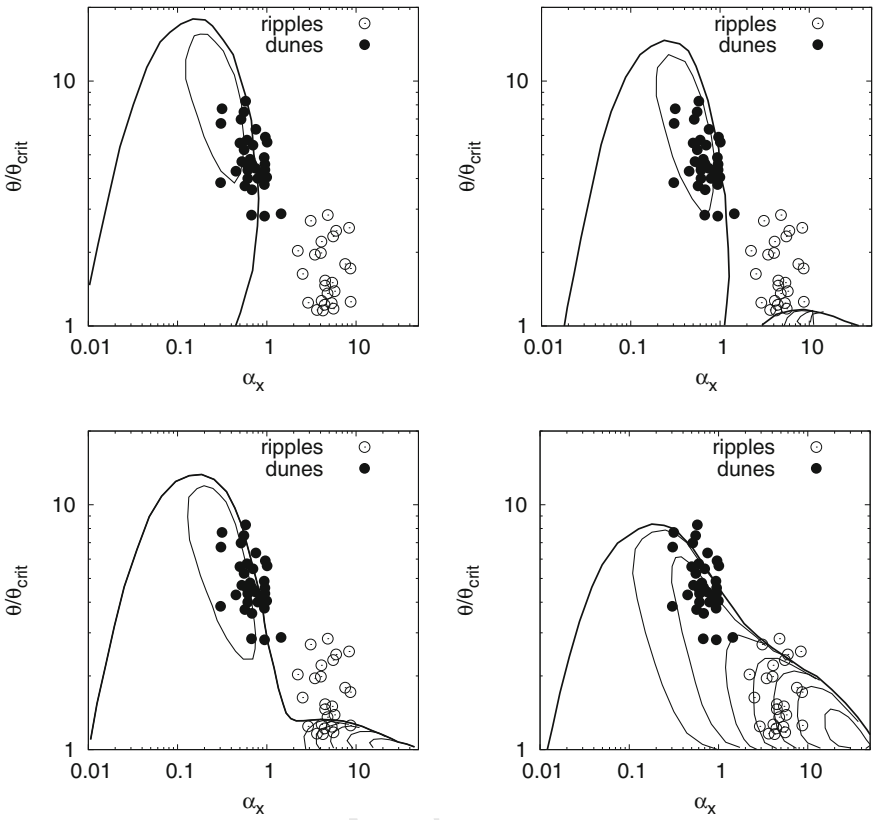

Fig. 2 Positive growth rate in the $(\alpha_x, \theta/\theta_{crit})$-plane. The thick line indicates the isoline characterized by vanishing values of Γ_r. **a** $R_p = 20$, **b** $R_p = 14$, **c** $R_p = 12$, **d** $R_p = 5$. The dots indicate the experimental data of Guy, Simons and Richardson (1966), 'Summary of alluvial channel data from flume experiments, 1956–61', US Government Printing Office

2.2 *Sand Waves*

Sand waves are large scale bottom undulations characterized by wavelengths of the order of hundreds of metres with crests almost orthogonal to the direction of the tidal current. One of the first contributions to the study of the mechanism that leads to the appearance of sand waves was given by Hulscher [17], who showed that the appearance of these bedforms is driven by the presence of steady recirculating cells generated by the interaction of the oscillatory tidal current with the bottom waviness. Hulscher [17] quantified turbulence mixing by introducing an eddy viscosity that is assumed to be constant over the water depth. Since the turbulence mixing tends to vanish close to a rigid wall, the model by Hulscher [17] neglects the bottom layer and introduces a partial slip condition of the fluid at the bottom. A more accurate model is that of Besio et al. [5], who used the approach proposed by Blondeaux and Vittori [8,

9] to evaluate the flow field. In particular, the turbulence generated by tidal currents was modelled by introducing an eddy viscosity that grows linearly with the distance from the bottom in the region close to the sea bottom, it reaches a maximum and it decreases and assumes small values close to the free surface. Moreover, since the analysis of Besio et al. [5] was aimed at studying both sand waves and sand banks and the dynamics of the latter bedforms is affected by Coriolis terms and the local time derivatives of the velocity components, Besio et al. [5] considered the contribution of these terms to the hydrodynamic problem.

Even though it is possible to consider tidal currents generated by the superposition of two or more tide constituents (e.g. semidiurnal and diurnal constituents), Besio et al. [5] assumed that the solution at the leading order of approximation was dominated by just one tide constituent, as made by Blondeaux et al. [10]. The solution of the hydrodynamic problem was obtained by expanding any unknown as a power series of ϵ. When terms of order ϵ of continuity and momentum equations were considered, partial differential linear equations for the flow and free surface perturbations were obtained. Since sediment continuity equation states that $dA(t^*)/dt^*$ is proportional to $A(t^*)$ through the ratio between the hydrodynamic and the morphodynamic time scales and this ratio turns out to be much smaller than one, the terms of the momentum equations that are proportional to the time derivative of $A(t^*)$ can be neglected with respect to the terms proportional to $A(t^*)$. Moreover, the periodicity of the basic flow suggests to write the unknown functions as Fourier series of time. By plugging the Fourier series into the hydrodynamic problem, a linear system of coupled ordinary differential equations can be derived, where the unknown functions depend only on the vertical coordinate. The solution can be numerically obtained with the procedure used by Vittori [33]. At last the equation, which provides the time development of the amplitude of the bottom perturbation, follows from the empirical predictors used to evalute the sediment transport rate and sediment continuity equation.

The results show that the bedforms, which tend to appear, are characterized by crests that are orthogonal to the major axis of the tidal ellipse. Indeed, the maximum value of the amplification rate is attained for vanishing values of $\alpha_{\hat{y}}$, $\hat{x}$ and $\hat{y}$ being two horizontal axes such that $\hat{x}$ is aligned with the major axis of the tidal ellipse. This theoretical finding agrees with field observations (see [1, 31]). Also the wavelength of the fastest growing mode predicted by their analysis agrees with the wavelength of the observed bottom forms. Moreover, since the velocity oscillations considered by Hulscher [17] and Besio et al. [5] are symmetric, the sand waves predicted by their stability analyses do not migrate. Later, Nemeth et al. [26] made a linear analysis similar to that of Hulscher [17] but they added a residual (steady) current to the main oscillatory tidal current. Hence, Nemeth et al. [26] found that the bedforms predicted by their analysis migrate in the direction of the steady current. However, field observations exist that show that sand waves can migrate also against the residual current. The migration of the bedforms in the direction opposite to that of the steady velocity component is possible because of the nonlinear relationship between the sediment trasport rate and the current velocity and it was investigated by Besio et al. [2, 3], who considered a tidal current generated by the superposition of the M2, M4 and Z0 constituents, which are supposed to be the dominant ones. The first two

constituents induce oscillations of the tidal current characterized by periods of about 12 and 6 h, respectively, while the Z0 constituent is characterized by a steady velocity component.

Up to now, only tidal currents which change on a temporal scale of the order of hours have been considered. However, the interaction between the lunar constituents with the solar constituents makes the tidal current to change also on much longer temporal scales, e.g. the temporal scale of the neap-spring cycle. As discussed in [10], the changes of the velocity field induced by a slow modulation of the tidal current can be determined, along with the time development of the bottom profile, if the presence of three distinct temporal scales is recognized. The first temporal scale is the tide period equal to $T_0^* = 2\pi/\omega^*$, which is of the order of hours. The second temporal scale is the period of the tide modulation equal to $T_1^* = 2\pi/\Omega_{sn}^* \cong 15$ days, Ω_{sn}^* being the angular frequency of the spring-neap cycle. The third and last temporal scale is the morphodynamic time scale $T_2^* = (1 - p_{or})h_0^{*2}/[d^*\sqrt{(\rho_s^*/\rho^* - 1)g^*d^*}]$, which depends on the local water depth and sediment characteristics (p_{or} is the porosity of the sea bottom). Considering their typical values, it appears reasonable to assume $T_0^* \ll T_1^* \ll T_2^*$ and to introduce the small parameters $\delta_1 = T_0^*/T_1^*$ and $\delta_2 = T_0^*/T_2^*$. Then, using a multiple scale approach [25], the following time variables, $t_0 = t = \omega^* t^*$, $t_1 = t^*/T_1^*$, $t_2 = t^*/T_2^*$ can be introduced and the unknown functions, which appear at the different orders of approximation ($O(\epsilon^0)$, $O(\epsilon)$, ...), are assumed to depend on t_0, t_1 and t_2 beside on the spatial coordinates. Sediment continuity equation suggests that A can be decomposed into a part of order one, which depends only on t_2, and a further contribution, which depends on t_0, t_1 and t_2 but it is much smaller than one: $A = A_0(t_2)\,[1 + \delta_2 A_1(t_0, t_1, t_2)]$. The function $A_0(t_2)$ describes the growth/decay of the bottom perturbation, which takes place on the morphodynamic time scale, whereas $A_1(t_0, t_1, \ldots)$ describes the oscillations of the bottom configuration, which take place during the tidal cycle and the spring-neap cycle. However, because of the small values of δ_2, the bottom oscillations described by A_1 are of small amplitude and can be neglected. Since significant bottom changes take place on the morphodynamic time scale t_2 only, the velocity and pressure fields can be assumed to respond instantaneously to the variations of the bottom configuration. Then, the equation that provides the time development of the amplitude of the bottom perturbation follows from sediment continuity equation. A comparison between the model findings and the characteristics of the sand waves observed in the North Sea was made by considering the data collected by Menninga [24]. A fair agreement among the theoretical predictions and the field observations was found. In particular, the analysis was able to predict the migration of the bedforms which is in the direction of the residual current or against it, depending on the strength of the different tide constituents.

2.3 Long Bed Waves

Long bed waves are periodic bottom forms characterized by a crest-to-crest distances, which are larger than those of sand waves and smaller than those of sand banks and, more importantly, by crests which form an angle with the direction of the tidal current, which ranges from about $-65°$ to about $35°$. Moreover, these bedforms are characterized by a morphodynamic time scale that is much longer than the period of the tide and significant changes of the bottom configuration take place only after a large number of tidal cycles. Therefore, it is convenient to introduce the two different time variables t_0 and t_2 already defined. Of course, the oscillations of the bottom profile during the tidal cycle have negligible effects and they can be safely neglected to determine the long term behaviour of the bottom configuration. The equation that provides the time development of the amplitude $A(t_2)$ of the generic component of the bottom perturbation follows from sediment continuity equation and it allows to discriminate the perturbation components which grow from those which decay and to evaluate the component characterized by the fastest growth. The model was tested against the field data described in [20] and fair results were obtained. Indeed, different relative maxima of $\overline{\Gamma}_r$ were identified and the predicted wavelengths well agree with the values of the different bedforms observed in the field. The presence of multiple relative maxima and the emergence of long bed waves appear to be related to the relative weakness of the tidal current, the ellipticity of the tidal current and the anisotropy of the slope-induced sediment transport. Indeed, for the same values of the parameters, but for stronger tidal velocities and/or unidirectional tidal currents and/or isotropic slope-induced sediment transport, the amplification rate Γ_r^* has only one significant maximum that corresponds to sand banks.

2.4 Sand Banks

Sand banks are large scale bottom forms that are characterized by crests that are almost aligned with the major axis of the tidal ellipse and by a crest-to-crest distance of the order of 10 km (see Fig. 3). To predict the appearance of sand banks and their geometrical characteristics two approaches were used. The first approach is based on the shallow water approximation whereas the second approach considers the full three-dimensional equations. First, we discuss the results that were obtained by means of the three-dimensional approach [5]. When the values of $\overline{\Gamma}_r^*$ are plotted versus the wavenumbers $(\alpha_{\hat{x}}, \alpha_{\hat{y}})$, for values of the hydrodynamic and morphodynamic parameters chosen to reproduce the site in the North Sea described in [22, 23], two maxima appear. One maximum describes sand waves and the other maximum describes sand banks. Indeed, field data collected along the Calais-Dover strait show that both sand waves and sand banks were observed in the site. The wavelength of the observed sand waves, which have crests practically orthogonal to the main tidal current, falls between 350 and 750 m and the sand banks are almost aligned with the

AQ1

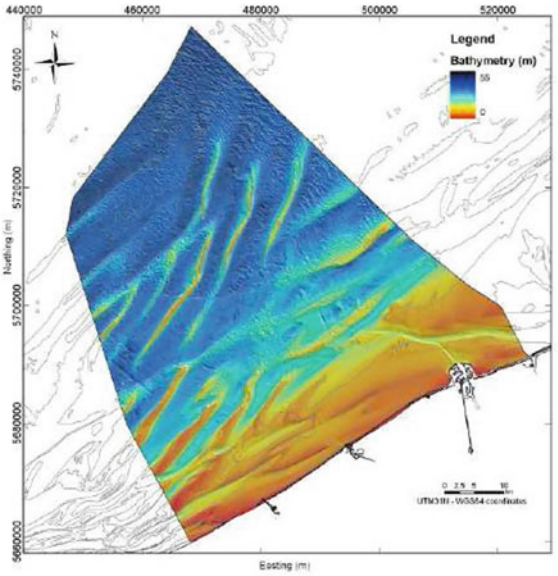

Fig. 3 The digital elevation model of the Belgian continental shelf based on single beam measurements (courtesy of Vera van Lancker)

main axis of the tidal ellipse but slightly clockwise rotated and are characterized by an average crest-to-crest distance of about 8 km. One of the maxima predicted by the model of Besio et al. [5] takes place for $\alpha_{\hat{x}} \simeq 0.38$ and a vanishing value of $\alpha_{\hat{y}}$. The second maximum takes place for $\alpha_{\hat{x}} = 0.013$ and $\alpha_{\hat{y}} = 0.03$. Hence, the stability analysis predicts the appearance of two different bedforms. The first bedform has crests orthogonal to the direction of the tidal current and its wavelength is about 355 m. The second bedform has crests slightly clockwise rotated with respect to the major axis of the tidal ellipse and its wavelength is about 5.5 Km. It is easy to associate the first mode to the sand waves observed by Le Bot et al. [22, 23] and the second mode to the sand banks that are present nearby (Sandettie bank, Ruytingen bank, Dyck bank).

Once it is verified that the three-dimensional approach provides reliable predictions of the tidal bedforms, let us look at the results provided by the shallow water approach. Hulscher et al. [18] were among the first investigators to study the process that leads to the appearance of sand banks by using the shallow water approximation. For a unidirectional tide, the fastest growing mode predicted by Hulscher et al. [18] is characterized by crests almost aligned with the main axis of the tidal ellipse and the wavelength of the predicted bedforms is in agreement with the field observations. However, the analysis of Hulscher et al. [18] shows that the first mode that becomes unstable, when the parameters are varied, corresponds to an ultra-long bottom form. Better predictions were found by Hulscher et al. [18] by considering circular tides. Indeed, the first mode to become unstable, when the parameters are varied, is characterized by a finite wavelength but, since a circular tide has no preferred direction,

no preferred orientation of the selected bedforms was provided by the theoretical analysis of Hulscher et al. [18].

Since a depth-averaged approach cannot predict the deviation of the sediment transport rate from the direction of the depth averaged velocity, Besio et al. [4] developed a model based on the shallow water approximation but they added a correction to the sediment transport direction to account for this three-dimensional effect. Moreover, the solution procedure used by Besio et al. [4] takes into account the cascade process that gives rise to a large number of harmonic components in the velocity field, that are generated by the interaction of the oscillatory tidal current with the bottom waviness. Finally, the approach proposed by Besio et al. [4] allows to consider unidirectional as well as elliptical and circular tides. When the real part $\overline{\Gamma}_r^*$ of the averaged amplification rate $\overline{\Gamma}^*$ is plotted versus $\alpha_{\hat{x}}^*$ and $\alpha_{\hat{y}}^*$, for a clockwise rotating tidal current, the most unstable perturbation generated by a circular tide has no preferred orientation. For a unidirectional tide, the crests of the most unstable mode are counter-clockwise rotated with respect to the direction of the tidal current. For values of the ratio e between the minor and major axes of the tidal ellipse falling between 0 and 1, the most unstable mode is always characterized by crests that are counter-clockwise rotated with respect to the main tidal current.

Of course the results obtained for the same values of the parameters but for a counter-clockwise rotating velocity vector do not differ from the previous ones when a unidirectional tide is considered. Moreover, for a circular tide only quantitative differences are present. However, for an elliptical tide, qualitative differences are present. In fact, for values of e falling between 0.02 and 0.6, the maximum of the amplification rate is characterized by positive values of both $\alpha_{\hat{x}}^*$ and $\alpha_{\hat{y}}^*$ and the predicted sand banks are clockwise rotated. Hence, the results obtained by Besio et al. [4] are in agreement with the findings of Besio et al. [5] and show that both a three dimensional analysis and a shallow water model predict the appearance of large scale bedforms, the orientation of which depends on the clockwise/counter-clockwise rotation of the tidal velocity vector.

Even though a linear stability analysis can predict the crest-to-crest distance and the orientation of sand banks, little is known on mechanism that leads to equilibrium conditions. The extension of the linear analysis made by Huthnance [19] provides an equilibrium profile of the sand banks but the hydrodynamics is described by a simplified approach. Roos et al. [29] developed a numerical approach that fully resolves the morphodynamics of the fastest growing mode. However, the numerical approach was applied only considering a unidirectional tidal current and the solution procedure implies significant computational costs.

A weakly nonlinear stability analysis is an alternative tool to determine the equilibrium profile attained by the unstable bottom perturbations when the parameters are close to their critical values. Indeed weakly nonlinear stability analyses have been successfully used in hydrodynamic stability and have been also applied to morphodynamic problems [12, 30, 34].

However, difficulties in the formulation of a weakly nonlinear stability analysis of the growth of sand banks for a unidirectional tidal current arose, because the first linear analyses predicted vanishing values of the wavenumber of the most unstable

mode close to the critical conditions. In other words, close to the critical conditions, the bottom forms predicted by the linear analyses were characterized by an infinite wavelength. This problem was overcame by Tambroni and Blondeaux [32] who employed a sediment transport predictor that provides vanishing values of the sediment transport rate when the bottom shear stress is smaller than its critical value. The introduction of a critical value of the Shields parameter allowed to obtain better predictions of the sediment transport rate and of the morphodynamic phenomena when the bottom shear stress is close to the initiation of sediment motion. In particular, close to the critical conditions and for tidal currents characterized by a low ellipticity, Tambroni and Blondeaux [32] found that the wavelength of the most unstable mode turns out to be finite. This result opened the possibility to carry out a weakly nonlinear stability analysis. The time development of the most unstable mode was determined by Tambroni and Blondeaux [32] for values of the parameters that differ from the critical ones by a small amount ε. For such values of the parameters, the bottom waviness turns out to be of order $\varepsilon^{1/2}$ and the amplitude of the most unstable component of the bottom perturbation is provided by

$$\frac{dA}{dt^*} = a_1^* A + a_2^* |A|^2 A. \tag{3}$$

Equation (3) is of Landau-Stuart type and can be integrated in closed form to obtain the time development of a small bottom perturbation and its equilibrium amplitude ($|A_{1e}| = \sqrt{-\text{Real}(a_1^*)/\text{Real}(a_2^*)}$).

3 Conclusions

Tidal currents flowing over a cohesionless sea bottom give rise to the formation of bedforms of different length scales ranging from tens of centimetres to tens of kilometres. Examples of these bedforms are ripples, megaripples, sand waves, long bed waves and sand banks. The results of stability analyses, which can predict the appearance of these bedforms and their main geometrical characteristics, are reviewed. Needless to write that the hydrodynamics is described assuming the flow regime to be turbulent and considering Reynolds equations either neglecting Coriolis effects, when the dynamics of small bedforms is analysed, or taking them into account, when the largest bedforms (e.g. sand banks) are analysed. The linear stability analyses provide reliable predictions of the wavelength and orientation of a large number of the periodic bedforms observed in tidal seas. In a few cases, a weakly nonlinear stability analysis can be used to estimate the equilibrium amplitude of the bedforms even though in many cases the equilibrium bottom configuration can be predicted only taking into account strong nonlinear effects and using a numerical approach.

References

1. Belderson, R.H., Johnson, M.A., Kenyon, N.H.: Bedforms. In: Stride, A.H. (Ed.) Offshore Tidal Sand, Processes and Deposits. Chapman & Hall (1982)
2. Besio, G., Blondeaux, P., Brocchini, M., Vittori, G.: Migrating sand waves. Ocean Dyn. **53**(3), 232–238 (2003)
3. Besio, G., Blondeaux, P., Brocchini, M., Vittori, G.: On the modeling of sand wave migration. J. Geophys. Res. Oceans **109**(C4) (2004)
4. Besio, G., Blondeaux, P., Vittori, G.: Sand bank formation: comparison between 2D and 3D models. In: 4th IAHR Symposium on River, Coastal and Estuarine Morphodynamics, Urbana, Illinois, October, 4–7 (2005)
5. Besio, G., Blondeaux, P., Vittori, G.: On the formation of sand waves and sand banks. J. Fluid Mech. **557**, 1–27 (2006)
6. Blondeaux, P., Colombini, M., Seminara, G., Vittori, G.: Introduction to Morphodynamics of Sedimentary Patterns, pp. 1–96. Genova University Press (2018)
7. Blondeaux, P., De Swart, H.E., Vittori, G.: Long bed waves in tidal seas: an idealized model. J. Fluid Mech. **636**, 485–495 (2009)
8. Blondeaux, P., Vittori, G.: Flow and sediment transport induced by tide propagation: 1. The flat bottom case. J. Geophys. Res. Oceans **110**(C7) (2005)
9. Blondeaux, P., Vittori, G.: Flow and sediment transport induced by tide propagation: 2. The wavy bottom case. J. Geophys. Res. Oceans **110**(C8) (2005)
10. Blondeaux, P., Vittori, G.: Formation of tidal sand waves: effects of the spring-neap cycle. J. Geophy. Res. Oceans **115**(C10) (2010)
11. Colombini, M.: Revisiting the linear theory of sand dune formation. J. Fluid Mech. **502**, 1–16 (2004)
12. Colombini, M., Seminara, G., Tubino, M.: Finite-amplitude alternate bars. J. Fluid Mech. **181**, 213–232 (1987)
13. Colombini, M., Stocchino, A.: Ripple and dune formation in rivers. J. Fluid Mech. **673**, 121–131 (2011)
14. Dyer, K.R., Huntley, D.A.: The origin, classification and modelling of sand banks and ridges. Cont. Shelf Res. **19**(10), 1285–1330 (1999)
15. Fourriere, A., Claudin, P., Andreotti, B.: Bedforms in a turbulent stream: formation of ripples by primary linear instability and of dunes by nonlinear pattern coarsening. J. Fluid Mech. **649**, 287–328 (2010)
16. Guy, H.P., Simons, D.B., Richardson, E.V.: Summary of Alluvial Channel Data from Flume Experiments, 1956–61, vol. 462. US Government Printing Office (1966)
17. Hulscher, S.J.M.H.: Tidal-induced large-scale regular bed form patterns in a three-dimensional shallow water model. J. Geophys. Res. Oceans **101**(C9), 20727–20744 (1996)
18. Hulscher, S.J.M.H., de Swart, H.E., de Vriend, H.J.: The generation of offshore tidal sand banks and sand waves. Cont. Shelf Res. **13**(11), 1183–1204 (1993)
19. Huthnance, J.M.: On the formation of sand banks of finite extent. Estuar. Coast. Shelf Sci. **15**(3), 277–299 (1982)
20. Knaapen, M.A.F., Hulscher, S.J.M.H., de Vriend, H.J., Stolk, A.D.: A new type of sea bed waves. Geophys. Res. Lett. **28**(7), 1323–1326 (2001)
21. LeBlond, P.H., Mysak, L.A.: Waves in the Ocean. Elsevier (1981)
22. Le Bot, S., Trentesaux, A., Garlan, T., Berne, S., Chamley, H.: Influence des tempêtes sur la mobilité des dunes tidales dans le détroit du Pas-de-Calais. Oceanol. Acta **23**(2), 129–141 (2000)
23. Le Bot, S., Idier, D., Garlan, T., Trentesaux, A., Astruc, D.: Dune dynamics: from field measurements to numerical modelling. Application to bathymetric survey frequency in the Calais-Dover Strait. Marine Sandwave Dyn. 101–108 (2000)
24. Menninga, P.J.: Analysis of variations in characteristics of sand waves observed in the Dutch coastal zone: a field and model study. Ph.D. Thesis, University of Utrecht (2012)

25. Nayfeh, H.: Perturbation Methods. Wiley (1973)
26. Németh, A.A., Hulscher, S.J.M.H., de Vriend, H.J.: Modelling sand wave migration in shallow shelf seas. Cont. Shelf Res. **22**(18–19), 2795–2806 (2002)
27. Raudkivi, A.J., Witte, H.H.: Development of bed features. J. Hydraulic Eng. **116**(9), 1063–1079 (1990)
28. Raudkivi, A.J.: Transition from ripples to dunes. J. Hydraulic Eng. **132**(12), 1316–1320 (2006)
29. Roos, P.C., Hulscher, S.J.M.H., Knaapen, M.A.F., Van Damme, R.M.J.: The cross-sectional shape of tidal sandbanks: modeling and observations. J. Geophys. Res. Earth Surface **109**(F2) (2004)
30. Schielen, R., Doelman, A., De Swart, H.E.: On the nonlinear dynamics of free bars in straight channels. J. Fluid Mech. **252**, 325–356 (1993)
31. Stride, A.H.: Offshore tidal deposits: sand sheet and sand bank facies. 95–125 (1982)
32. Tambroni, N., Blondeaux, P.: Sand banks of finite amplitude. J. Geophys. Res. Oceans **113**(C10) (2008)
33. Vittori, G.: Non-linear viscous oscillatory flow over a small amplitude wavy wall. J. Hydr. Res. **27**(2), 267–280 (1989)
34. Vittori, G., Blondeaux, P.: Sand ripples under sea waves Part 2: Finite-amplitude development. J. Fluid Mech. **218**, 19–39 (1990)
35. Vittori, G., Blondeaux, P.: River dunes and tidal sand waves: are they generated by the same physical mechanism? Water Resour. Res. **56**(5), e2019WR026800 (2020)

523780_1_En_21_Chapter ☑ TYPESET ☐ DISK ☐ LE ☑ CP Disp.:15/1/2022 Pages: xxx Layout: T1-Standard

Author Queries

Chapter 21

Query Refs.	Details Required	Author's response
AQ1	Please provide high-resolution source file for Fig. 3.	
AQ2	References [7, 14, 27, 28] are given in the list but not cited in the text. Please cite them in text or delete them from the list.	

MARKED PROOF

Please correct and return this set

Please use the proof correction marks shown below for all alterations and corrections. If you wish to return your proof by fax you should ensure that all amendments are written clearly in dark ink and are made well within the page margins.

Instruction to printer	*Textual mark*	*Marginal mark*
Leave unchanged	··· under matter to remain	New matter followed by
Insert in text the matter indicated in the margin		or (x2)
Delete	through single character, rule or underline or through all characters to be deleted	or (x2)
Substitute character or substitute part of one or more word(s)	through letter or through characters	new character or new characters
Change to italics	under matter to be changed	
Change to capitals	under matter to be changed	
Change to small capitals	under matter to be changed	
Change to bold type	under matter to be changed	
Change to bold italic	under matter to be changed	
Change to lower case	Encircle matter to be changed	
Change italic to upright type	(As above)	
Change bold to non-bold type	(As above)	
Insert 'superior' character	through character or where required	or under character e.g. or
Insert 'inferior' character	(As above)	over character e.g.
Insert full stop	(As above)	
Insert comma	(As above)	
Insert single quotation marks	(As above)	or and/or or
Insert double quotation marks	(As above)	or and/or or
Insert hyphen	(As above)	
Start new paragraph		
No new paragraph		
Transpose		
Close up	linking characters	
Insert or substitute space between characters or words	through character or where required	
Reduce space between characters or words	between characters or words affected	